

Hypersonic Glider Autopilot Using Adaptive Higher Order Sliding Mode Control with Impulsive Actions

Christian Tournes^{1,*}, Yuri Shtessel², Allen Spencer¹

¹Aero Thermo Technology Inc., Huntsville, USA

²Department of Electrical and Computer Engineering, University of Alabama in Huntsville, Huntsville, USA

Email address:

Christian.Tournes@Aerothermo.com (C. Tournes), shtessy@uah.edu (Y. Shtessel), Allen.Spencer@aerothermo.com (A. Spencer)

*Corresponding author

To cite this article:

Christian Tournes, Yuri Shtessel, Allen Spencer. Hypersonic Glider Autopilot Using Adaptive Higher Order Sliding Mode Control with Impulsive Actions. *American Journal of Aerospace Engineering*. Vol. 5, No. 2, 2018, pp. 71-86. doi: 10.11648/j.ajae.20180502.12

Received: August 28, 2018; **Accepted:** September 14, 2018; **Published:** October 25, 2018

Abstract: Hypersonic glider designs often exhibit limited control authority and poor transversal stability. Furthermore, the methods used for aerodynamic performance estimation at high flight altitudes and hypersonic speeds are inevitably inaccurate and uncertain. Hypersonic Glider performance could be severely degraded by using traditional control and autopilot techniques that rely on an accurate knowledge of the aerodynamic coefficients. A new autopilot and control approach, presented in this paper, is based on recently developed special Higher Order Sliding Mode Control (HOSMC) algorithms that are mostly based on relative degrees but not on the glider's mathematical model. Specifically, this autopilot and control approach includes robust continuous aerodynamic control augmented by impulsive reaction control thrusters. Control gain-adaptation allows addressing the vehicle bounded uncertainties and perturbations without overestimating the control gains. The impulsive augmentation of the continuous Higher Order Sliding Mode control provides almost instantaneous convergence thereby mitigating the risk of control loss caused by sideslip angle departures due to poor transversal stability and small lateral control authority. While Higher Order Sliding Mode control algorithms are inherently insensitive to the matched uncertainties and disturbances, the observers embedded in the Continuous Higher Order Sliding Mode Control algorithms reduce the time response of the control compensation. Simulation of a representative hypersonic glider executing normal and bank-to-turn maneuvers and controlled by the studied algorithms demonstrate excellent performance in the presence of significant model uncertainties and perturbations.

Keywords: Hypersonic Gliders, Autopilots, Higher Order Sliding Mode Control

1. Introduction

Controlling hypersonic vehicles, whether propelled or not presents several serious challenges. To reduce drag and aerodynamic heating, hypersonic glider control surfaces are reduced as much as possible which adversely affects the corresponding control authority. Given very large velocity magnitude, the dampening by roll, pitch and yaw rates is mediocre and the slenderness of the body results in a very poor lateral stability. Traditional, aerodynamic model based control techniques are only as good as the models themselves. Specifically, aerodynamic coefficient uncertainties and perturbations yield complications in obtaining an accurate mathematical model of the hypersonic

glider control response. Furthermore, obtaining accurate dynamical models is difficult given the flight conditions considered, the extreme temperatures, possible mix of laminar and turbulent boundary layer and possible non-continuous flow conditions. The problem is compounded with ablation phenomena that modify the shape of the body, modify the position of the center of gravity and introduce chemical reactions into the flow. During cruise flight the hypersonic glider bank to turn maneuvers are infrequent and the cruising maneuvers can be made relatively slow to minimize the occurrence of excessively large sideslip angle transients. However, during terminal maneuvers they may also have to include a fast half roll maneuver aimed at driving the flight path angle from a small negative cruising value to large terminal dive angle. During terminal

maneuvers, the sideslip angle may be prone to exhibiting one or several significant transient overshoots possibly resulting in loss of control.

The *modus operandi* of the art aerodynamically steered vehicles is that the trajectory is controlled via a two-loop feedback by commanding aerodynamic angles that is, angle of attack and sideslip angle for skid-to-turn configured vehicles or angle of attack, roll angle and nullified sideslip angle for bank-to-turn vehicles. As a result, the trajectory is controlled by an outer-loop autopilot that uses commanded aerodynamic accelerations as pseudo controls. An inversion algorithm calculates body attitude maneuvers conducive to producing commanded acceleration and finally, an inner loop sets the corresponding aerodynamic angles using the attitude control surfaces. With this *modus operandi*, model uncertainties exert a detrimental effect on the accuracy of the inversion.

A control-oriented model of a hypersonic vehicle with curve-fitted approximations of the aerodynamic forces and moments [1] may be used for robust controller design. Then, an adaptation technique may be employed for estimating unknown constant coefficients used in the approximations [2]. Unfortunately, in the presence of time-varying nonlinear uncertain coefficients, the accuracy of the control adaptation can be compromised. Therefore, the design of hypersonic gliders control laws robust enough to handle significant model uncertainties still represents a challenging task. Possible control solutions may be based on back-stepping techniques [3], dynamic inversion [4] or Higher Order Sliding Mode (HOSM) control [5] combined with filters used to shape desired flight qualities and to calculate the stability derivatives of commanded aerodynamic angles. Higher Order Sliding Mode (HOSM) control [6-8], being insensitive to the matched bounded additive and multiplicative perturbations, constitutes a very attractive control technology that does not rely on an imbedded dynamical model but only requires knowledge of relative degree. Thus, the HOSM approach can address the challenges in hypersonic glider control. To date, HOSM control and observation techniques have been effectively applied for missile-interceptor integrated guidance and autopilot control [9-10] while mitigating the discussed challenges. The proposed Continuous Adaptive HOSM and observation techniques were also used for controlling an air-breathing hypersonic missile in a terminal phase [11].

The important enduring problems are first, that hypersonic vehicles experience ablation during the flight which causes poorly predictable variations of a shape and modifications of the position of the gravity center which may result in a large disturbance. The problem is aggravated by limited control authority that precludes operating with large autopilot gains. Although during the cruise phase most maneuvers are slow, at the end of the cruise, the vehicle may have to undergo large amplitude roll maneuvers which may induce large variations of sideslip angle. There is a clear need for a control law design that prevents the sideslip angle from exceeding maximum controllable magnitudes and that reduces as much as possible the duration of any corresponding sideslip angle

transients.

A possible approach for addressing inherent robustness issues is H_∞ as proposed in [12], observers can be used for providing fault tolerant designs [13]. Since dynamic pressure is a major parameter in the calculation of aerodynamic stability derivatives it may be applied to provide a gain scheduling basis as in [14]. Gyroscopes may also be used to providing moment control [15].

The challenges described above are addressed in this work using the recently proposed Continuous Adaptive HOSM control algorithm [11-16]. The proposed algorithm accommodates the use of impulsive (thrust) control actions [19-24] for achieving faster convergence. Specifically, in this work it is proposed to use the Adaptive Continuous Higher Order Sliding Mode control [7, 16] with the impulsive action [22-24] for controlling a hypersonic glider. Continuous Adaptive HOSM control comprises a Continuous Finite Time Convergent Control [7, 16] that operates in a concert with the HOSM disturbance observer [6-7] designed to cope with external disturbances and model uncertainties which include multiplicative aerodynamic model errors. An improvement to this design includes a gain adaptation algorithm [16] that is based on the concept of Equivalent Control, which yields an adaptive gain that closely follows the disturbance. This disturbance avoids overestimating the gain and reduces possible chattering effects which may be caused by unmodeled (actuator) dynamics.

The use of impulsive control in concert with the Continuous Adaptive HOSM is studied in this paper for improving the control of the sideslip angle of the hypersonic glider, especially when engaging in aggressive bank-to-turn maneuvers. The interest for impulsive control aimed at driving the system's states to the origin in a timely fashion has grown in recent years as in [19-24]. Since the shaping of the pulse sequence is calculated based on the nominal model, it does not account for the thruster's dynamics and does not account for disturbances and it is thus, inherently inaccurate and not robust if used alone. For that matter hybrid-impulsive solutions have been studied as in [22-23] aimed at reducing dramatically the convergence time and improving uniformity [6-7]. The impulsive control is implemented in this design via a pair of yaw attitude thrusters which provides almost instantaneous convergence of the sideslip angle to the origin in less than 0.4 sec. In this study, impulsive control is associated with Continuous Adaptive HOSM where the initial approximate dead beat is to be followed by the corresponding Continuous Adaptive HOSM operation which achieves the perfect robustness to the matched perturbations. Here, the impulsive control is implemented as a sequence of Dirac delta-function and its derivatives represented by their approximations as in [23-25]. Impulsive algorithm calculates the sequence of impulses which drives initial states to the origin in a very short time. Note that inevitable model inaccuracies could preclude impulsive control algorithm to from perfectly converging to the origin and only to the vicinity of the origin. This does not present a significant problem, since upon completion of impulsive control the

Adaptive HOSM control takes over and provides the required robustness and the finite time convergence.

The paper is structured as follows: Section 2 presents the developed method and, for that matter, contains a background of Adaptive HOSM-Impulsive Control and second order SMC based on Nonlinear Dynamic Sliding Manifold (NDSM) that is described in Sub-section 2.1. Sub-section 2.2 presents the mathematical model of a hypersonic glider and the statement of the problems. Sub-section 2.3 presents NDSM baseline controller design used as a basis of comparison with the designs developed in this work. Continuous Fixed Parameters HOSM control is studied in Sub-section 2.4, while Sub-section 2.5 presents the design of Continuous Adaptive HOSM control. The study of yaw impulsive control associated with Continuous HOSM control is presented in Sub-section 2.6. Simulation results are presented in Section 3 and are discussed in Section 4, followed by Conclusion

2. Method

2.1. Background of Adaptive Higher Order Sliding Mode and Impulsive Control

2.1.1. Continuous Higher Order Sliding Mode Control

Consider a Single Input, Single Output (SISO) input-output dynamics of the form [11]

$$\sigma^{(r)} = f(x, t) + u \quad (1)$$

where $u \in \mathbb{R}^1$, $\sigma \in \mathbb{R}^1$ are the control and output (sliding) variables, respectively, and $f(x, t)$ is an unknown disturbance with a bounded derivative. The following theorem gives a control law that provides finite time convergence in the unperturbed version of system (1).

Theorem 1 [17] Consider the unperturbed system (1) with $f(x, t) \equiv 0$. Let the $\gamma_i > 0$ be the coefficients of the Hurwitz polynomial $s^r + \gamma_r s^{r-1} + \dots + \gamma_2 s + \gamma_1$ then, there exists $\varepsilon \in (0, 1)$ such that for every $a \in (1 - \varepsilon, 1)$ the origin of the system (1), $\sigma = \dot{\sigma} = \dots = \sigma^{(r-1)} = 0$ is a globally finite-time stable equilibrium under the feedback control

$$u = -\gamma_r |\sigma^{(r-1)}|^{a_r} \text{sign}(\sigma^{(r-1)}) - \gamma_{r-1} |\sigma^{(r-2)}|^{a_{r-1}} \text{sign}(\sigma^{(r-2)}) - \dots - \gamma_1 |\sigma|^{a_1} \text{sign}(\sigma) \quad (2)$$

where the coefficients a_1, a_2, \dots, a_r satisfy

$$a_{i-1} = \frac{a_i a_{i+1}}{2a_{i+1} - a_i}, \quad i = 2, \dots, r \quad (3)$$

with $a_{r+1} = 1$, $a_r = a$.

Remark 1: The control (1-3) is continuous.

Remark 2: Theorem 1 is clearly an existence theorem and the gains a_i may be computed by simulation like in [6, 7]. Equation (4) below shows an example of a set of gains which satisfies the conditions of Theorem 1 and achieves finite time convergence for systems of order up to 4 with the roots of the

polynomial $s^r + \gamma_r s^{r-1} + \dots + \gamma_2 s + \gamma_1$ all equal to -2 .

$$\begin{aligned} r=1; \quad u &= -2|\sigma|^{1/2} \text{sign}(\sigma) \\ r=2; \quad u &= -4|\dot{\sigma}|^{3/5} \text{sign}(\dot{\sigma}) - 4|\sigma|^{3/7} \text{sign}(\sigma) \\ r=3; \quad u &= -6|\ddot{\sigma}|^{7/10} \text{sign}(\ddot{\sigma}) - 12|\dot{\sigma}|^{7/13} \text{sign}(\dot{\sigma}) \\ &\quad - 8|\sigma|^{7/16} \text{sign}(\sigma) \\ r=4; \quad u &= -8|\ddot{\sigma}|^{4/5} \text{sign}(\ddot{\sigma}) - 24|\dot{\sigma}|^{2/3} \text{sign}(\dot{\sigma}) \\ &\quad - 32|\sigma|^{4/7} \text{sign}(\sigma) - 16|\sigma|^{1/2} \text{sign}(\sigma) \end{aligned} \quad (4)$$

The theoretical result that allows the design of a finite-time converging continuous control for the perturbed system (1) is formulated in the following theorem:

Theorem 2 [16]: Consider the perturbed system (1) with the smooth disturbance $f(x, t) \neq 0$ so that $|\dot{f}(x, t)| \leq H$, $H > 0$.

Let $\gamma_i > 0$ be the coefficients of the Hurwitz polynomial $s^r + \gamma_r s^{r-1} + \dots + \gamma_2 s + \gamma_1$ and $\varepsilon \in (0, 1)$ is identified so that the unperturbed system (1) is finite-time convergent with the control feedback (2-3) then, the origin of the perturbed system (1), $\sigma = \dot{\sigma} = \dots = \sigma^{(r-1)} = 0$ is a globally finite-time stable equilibrium under the continuous HOSM control:

$$u = -\gamma_r |\sigma^{(r-1)}|^{a_r} \text{sign}(\sigma^{(r-1)}) - \gamma_{r-1} |\sigma^{(r-2)}|^{a_{r-1}} \text{sign}(\sigma^{(r-2)}) - \dots - \gamma_1 |\sigma|^{a_1} \text{sign}(\sigma) - \lambda \quad (5)$$

where

$$\lambda = \eta_1 |s|^{1/2} \text{sign}(s) + \xi \quad (6)$$

$$\xi = \eta_2 \text{sign}(s), \quad \eta_1 = 1.5H^{1/2}, \quad \eta_2 = 1.1H$$

$$s = \sigma^{(r-1)} + z, \quad \dot{z} = -u - \lambda \quad (7)$$

Remark 3: The injection term λ in (6-7) represents a super-twisting observer [7, 8] that exactly reconstructs the smooth disturbance $f(x, t)$ with the bounded derivative in finite time.

2.1.2. Adaptive Continuous Higher Order Sliding Mode Control

If the bound $H > 0$ in the inequality, $|\dot{f}(x, t)| \leq H$, exists but is unknown then the overestimation of H may result in the overestimation of the control gains η_1 and η_2 in (6-7). As result, with this gain overestimation, un-modeled (actuator) dynamics can yield increased chattering. To reduce this possible chattering in the super-twisting observer (6-7), it is beneficial to design an adaptive-gain algorithm with does not overestimate the gains. Therefore, assuming that the gain η_1 can be selected large enough, the aim is to adapt η_2 in (6) so that $k(t) = \eta_2$ is close to H while satisfying the condition $k(t) = \eta_2 > H$. This self-tuning procedure reduces the amplitude of the high frequency switching part of the super-twisting term (6) which then mitigates chattering. In this paper an adaptive scheme built on the equivalent control [7, 16] is employed. The main result is formulated in the

following theorem:

Theorem 3 [11, 16]: Consider the system (1) with a twice differentiable disturbance $f(x, t)$ satisfying $|\dot{f}(x, t)| \leq H$, $|\ddot{f}(x, t)| \leq N$, assume $H > 0$ is unknown and $N > 0$ is known and let $\gamma_i > 0$ be such that the polynomial $s^r + \gamma_r s^{r-1} + \dots + \gamma_2 s + \gamma_1$ is Hurwitz. Then, there exists an $\varepsilon \in (0, 1)$ such that for every $a \in (1 - \varepsilon, 1)$ the origin $\sigma = \dot{\sigma} = \dots = \sigma^{(r)} = 0$ is a finite time stable equilibrium under the Adaptive Continuous HOSM control in (5), where a_1, a_2, \dots, a_r satisfy (3-4) with $a_{r+1} = 1$, $a_r = a$ and λ is defined in

$$\begin{aligned} \lambda &= \eta_1 |s|^{1/2} \text{sign}(s) + w \\ \dot{w} &= k(t) \text{sign}(s) \end{aligned} \quad (8)$$

where the adaptive gain $k(t)$ is computed in accordance with the following double-layer adaptation algorithm

$$\dot{k}(t) = -(\rho_0 + \rho(t)) \text{sign}(v(t)), \quad \rho_0 > 0 \quad (9)$$

$$v(t) = k(t) - \frac{1}{\varepsilon_1} |w_{eq}(t)| - \varepsilon_0 \quad (10)$$

$$\dot{\rho}(t) = \bar{\gamma} |v(t)| + \rho_0 \sqrt{\bar{\gamma}} \text{sign}(e(t)), \quad \gamma > 0 \quad (11)$$

$$e(t) = \frac{N}{\varepsilon_1} - v(t) \quad (12)$$

where $\bar{\gamma} > 0$, $0 < \varepsilon_1 < 1$, and $\varepsilon_0 > 0$ is a small real number and where $w_{eq}(t)$ is an equivalent control of $w(t)$ in (8) that can be estimated by $\hat{w}_{eq}(t)$ via low pass filtering:

$$\hat{w}_{eq}(t) = \text{LowPassFiltering}(w(t)) \quad (13)$$

Remark 4: When the value N exists, but is unknown (11) is simplified as [11, 16]

$$\dot{\rho}(t) = \bar{\gamma} |v(t)|, \quad \bar{\gamma} > 0 \quad (14)$$

2.1.3. Hybrid Continuous HOSM-Impulsive Control

The impulsive control based on the use of delta-functions and its derivatives allows driving the sliding set $\sigma, \dot{\sigma}, \dots, \sigma^{(r-1)}$ of (1) to the origin in a timely fashion, where the delta function and its derivatives are approximately implemented as in [22, 24]. This algorithm can be used in Reaction Control Systems (RCS) of aerospace vehicles including hypersonic gliders. This result is formulated in the following proposition:

Theorem 4 [22]: Consider system (1). Assume that

(A1) The initial conditions $\sigma(0), \dot{\sigma}(0), \dots, \sigma^{(r-1)}(0)$ in system (1) are available,

(A2) The delta function $\delta(t)$ and its $r-1$ derivatives

$\dot{\delta}(t), \ddot{\delta}(t), \dots, \delta^{(r-1)}(t)$ are exactly implementable and thus, the impulsive control law (15) drives $\sigma, \dot{\sigma}, \dots, \sigma^{(r-1)} \rightarrow 0$ in a timely fashion

$$u_{imp} = - \sum_{k=0}^{r-1} \sigma^{(r-k)}(0) \delta_{\varepsilon}^{(k)}(t) \quad (15)$$

where $\delta_{\varepsilon}^{(k)}$ are the generalized derivatives of the Dirac-delta distribution centered in $\varepsilon > 0$ defined as [24-25] with

$$\int \delta_{\varepsilon}^{(k)}(t) \phi(t) dt = (-1)^k \phi^{(k)}(\varepsilon) \quad (16)$$

Theorem 5 [22]: Consider the system (1) with a twice differentiable disturbance $f(x, t)$ satisfying $|\dot{f}(x, t)| \leq H$, $|\ddot{f}(x, t)| \leq N$, $H > 0$, $N > 0$. Assume that assumptions A1 and A2 hold, then the hybrid-impulsive continuous HOSM control is

$$u = v + u_{imp} \quad (17)$$

Where v is designed in a continuous HOSM control format (5-7) and is given by

$$v = -\gamma_r |\sigma^{(r-1)}|^{a_r} \text{sign}(\sigma^{(r-1)}) - \gamma_{r-1} |\sigma^{(r-2)}|^{a_{r-1}} \text{sign}(\sigma^{(r-2)}) - \dots - \gamma_1 |\sigma|^{a_1} \text{sign}(\sigma) - \lambda \quad (18)$$

with injection term λ defined in (6-7), v_{imp} is the impulsive control in (15) that drives $\sigma, \dot{\sigma}, \dots, \sigma^{(r-1)} \rightarrow 0$ in a timely fashion and after the finite time transient response the algorithm keeps the sliding variable and its time derivatives at the origin in the presence of disturbances.

Remark 5: The delta function and its derivative need to be approximated to make the impulsive control law (15) implementable for the RCS. The implementation issues are studied in [23-25].

Remark 6: The calculation of the impulses assume that corresponding aerodynamic controls are not used during the impulses and likewise it does not consider the coupling effects from control of the roll angle; while yaw aerodynamic controls are effectively not applied by design during the impulses, the associated coupling terms from roll control are exerted which may prevent the impulsive solution from being perfectly exact.

2.2. Mathematical Model and Problem Formulation

2.2.1. Dynamical Model

The vehicle dynamics are resolved in a frame obtained by rotating the NED frame [26] by the ground track angle χ ; they are governed by (19) hereafter where $\gamma, \chi, h, \mu, v_R$ represent respectively the flight path, ground track air path angle, height and velocity magnitude with respect to Earth, X, Y, Z represent non-inertial forces in wind axes and m is vehicle mass. Inertial accelerations are represented using the concept of quadratic relative gravity as in [27] with the term ξ .

$$\begin{aligned}
\dot{\gamma} &= \frac{Z \cos(\mu)}{mv_R} - \frac{Y \sin(\mu) \cos(\beta)}{mv_R} - \frac{g \xi_z}{v_R} \\
\dot{\chi}' &= \frac{Z \sin(\mu)}{mv_R \cos(\gamma)} + \frac{Y \cos(\mu) \cos(\beta)}{mv_R \cos(\gamma)} - \frac{g \xi_y}{v_R \cos(\gamma)} \\
\dot{v}_R &= -X/m - g \xi_x \\
\dot{h} &= v_R \sin(\gamma); \quad \mu = \tan^{-1} (v_R \cos(\gamma) (\dot{\chi} + g \xi_y) / (v_R \dot{\gamma} + g \xi_z)) \\
\begin{bmatrix} \xi_x \\ \xi_y \\ \xi_z \end{bmatrix} &= \mathbf{A} \begin{bmatrix} \bar{v}^2 \\ \bar{v} \\ 1 \end{bmatrix}
\end{aligned} \quad (19)$$

With

$$\begin{aligned}
A_{0,0} &= 0; A_{0,1} = 0; A_{2,0} = -\cos(\gamma) / \bar{r}' \\
A_{1,1} &= 2\bar{\omega}_{\oplus} [\sin(\gamma) \cos(\chi) \cos(L_{gC}) - \cos(\gamma) \sin(L_{gC})] \\
A_{2,1} &= -2\bar{\omega}_{\oplus} \sin(\chi) \cos(L_{gC}) \\
A_{0,2} &= [\sin(\gamma) g_c - g_N \cos(\gamma) \cos(\chi)].. \\
&+ \bar{\omega}_{\oplus}^2 (C_{\oplus} + \bar{h}) \cos(L_{gC}) [\cos(\gamma) \cos(\chi) \sin(L_{gC}).. \\
&- \cos(L_{gC}) \sin(\gamma)] \\
A_{1,2} &= -\sin(\chi) \{ \bar{\omega}_{\oplus}^2 \cos(L_{gD}) \sin(L_{gD}) (C_{\oplus} + \bar{h}) - g_N \} \\
A_{2,2} &= -\bar{\omega}_{\oplus}^2 (C_{\oplus} + \bar{h}) \cos(L_{gC}) [\cos(\gamma) \cos(L_{gC}).. \\
&+ \sin(\gamma) \cos(\chi) \sin(L_{gC})].. \\
&+ \sin(\gamma) \cos(\chi) g_N + \cos(\gamma) g_c
\end{aligned} \quad (20)$$

where $C_{\oplus} = (1 - e_{2\oplus} \sin(L_{gD}))^2)^{-1/2}$ [28], L_{gC} , L_{gD} represent geocentric and geodetic latitudes, r_{\oplus} , v_{\oplus} , t_{\oplus} are normalized length, velocity and time, $g = v_{\oplus} / t_{\oplus}$ is acceleration normalization factor commensurate with gravity and e_{\oplus} , $e_{2\oplus}$ are Earth's oblateness coefficients with $e_{2\oplus} = 2e_{\oplus} - e_{\oplus}^2$ and $e_{\oplus} = 1/298.257$

Normalized vertical component of gravity is according to [29] $g_c = 1/\bar{r}'^2 - 1.5J_2((3\sin(L_{gC})^2 - 1)/\bar{r}'^4$ and the "North" component of gravity is $g_N = -3J_2 \cos(L_{gC}) \sin(L_{gC}) / \bar{r}'^4$. Local curvature of the trajectory is defined [30] as:

$$1/\bar{r}' = 1 - \bar{h} - e_{\oplus} \sin(L_{gC})^2 + 2e_{\oplus} \cos(L_{gC})^2 \cos(\chi)^2.$$

Normalized radius from Earth's center and relative velocity magnitude are \bar{r} , \bar{v} and J_2 represents the second gravitational coefficient.

The upper bar represents normalized variables while the under bar represents average value of such variables during the scenario. Angle χ' represents the rotation rate of the projection of the velocity vector onto local horizontal plane, with respect to some constant reference vector. As consequence of vehicle relative velocity with respect to Earth, NED frame rotates around Down axis with angular rate (15) and so does the North axis of NED frame and

evidently $\dot{\chi} = \dot{\chi}' + \Delta\dot{\chi}$.

$$\Delta\dot{\chi} = v_R \cos(\gamma) \cos(\chi) \tan(L_{gD}) / \bar{r} \quad (21)$$

The formulation of [24] is like [29] with the difference that proposed formulation accounts for the Earth's oblateness as in [30] and the introduction of "relative" gravity term ξ as in [27] allows extending the use of the equations which represent flight over flat non-rotating Earth to oblate rotating Earth*.

Remark 7: As term ξ is represented as a second order polynomial function of relative velocity magnitude it is the base of the closed-form calculation of range and flight times as functions of initial and terminal velocities [27].

Aerodynamic forces X, Y, Z along the air path axis system as in [26] are defined by

$$\begin{aligned}
Z &= QS \{ c_{Z\alpha} \alpha + c_{z_{\delta m}} \delta_m \}; \quad Q = 0.5 \rho v_R^2 \\
Y &= QS \{ c_{Y\beta} \beta + c_{Y_{\delta n}} \delta_n + c_{Y_{\delta l}} \delta_l + c_{Y_{\Delta n}} \Delta_n \} \\
X &= QSc_X(\alpha, \delta_m)
\end{aligned} \quad (22)$$

Where Q, S, b, L_{ref}, ρ represent dynamic pressure, reference surface, span, reference chord and air density, $\delta_l, \delta_m, \delta_n$ control surfaces positions relative to maximum, $\alpha, \beta, \phi, \theta$ are the angle of attack, sideslip, roll and pitch angles, Δ_n represents yaw thruster impulsive control relative to maximum and finally $c_{[.]_0}$ represent linearized coefficients along $[.] = X, Y, Z$ caused by $(.) = l, m, n$; roll, pitch and yaw actuators. Given the large longitudinal velocity, acceleration damping effects caused by attitude motion are neglected in (22).

Combining (19-21) and introducing stability derivatives in (19) we obtain:

$$\begin{aligned}
\dot{\gamma} &= \cos(\mu) Z_{\alpha} \alpha + \cos(\mu) Z_{\delta m} \delta_m - g \xi_z / v_R - \sin(\mu) Y_{\beta} \beta.. \\
&.... - \sin(\mu) Y_{\delta n} \delta_n - \sin(\mu) Y_{\delta l} \delta_l - \sin(\mu) Y_{\delta l} \delta_l - \sin(\mu) Y_{\Delta n} \Delta_n \\
\dot{\chi} &= \frac{\sin(\mu)}{\cos(\gamma)} Z_{\alpha} \alpha + \frac{\sin(\mu)}{\cos(\gamma)} Z_{\delta m} \delta_m + \frac{\cos(\mu)}{\cos(\gamma)} Y_{\beta} \beta + \frac{\cos(\mu)}{\cos(\gamma)} Y_{\delta n} \delta_n \\
&.... - \frac{g \xi_y}{v_R \cos(\gamma)} + \frac{\cos(\mu)}{\cos(\gamma)} Y_{\delta l} \delta_l + \frac{\cos(\mu)}{\cos(\gamma)} Y_{\delta l} \delta_l + \frac{\cos(\mu)}{\cos(\gamma)} Y_{\Delta n} \Delta_n
\end{aligned} \quad (23)$$

Likewise yaw, pitch and roll Euler angle ψ, θ, ϕ dynamics and body rates p, q, r are given by

$$\begin{aligned}
\dot{\phi} &= p + q \sin(\phi) \tan(\theta) + r \cos(\phi) \tan(\theta) \\
\dot{\theta} &= q \cos(\phi) - r \sin(\phi) \\
\dot{\psi} &= \frac{q \sin(\phi) + r \cos(\phi)}{\cos(\theta)}
\end{aligned} \quad (24)$$

* The local frame is oriented with the "Down" vector directed to the center of Earth and not parallel to "local" horizontal

The dynamics of body rates p, q, r are given by [31] with L, N, M defined hereafter by (25) and c_j ; $j = 1..9$ defined by (26)

$$\begin{aligned}\dot{p} &= (c_1 r + c_2 p)q + c_3 L + c_4 N \\ \dot{q} &= c_5 p r - c_6 (p^2 - r^2) + c_7 M \\ \dot{r} &= (c_8 p - c_2 r)q + c_4 L + c_9 N\end{aligned}\quad (25)$$

$$\begin{aligned}\Gamma c_1 &= (J_y - J_z)J_z - J_{xz}^2; \quad \Gamma c_2 = (J_x - J_y + J_z)J_{xz}; \\ \Gamma c_3 &= J_z; \Gamma c_4 = J_{xz}; \quad c_5 = (J_z - J_x)/J_y; \\ c_6 &= J_{xz}/J_y; c_7 = 1/J_y; \Gamma c_8 = (J_x - J_y)J_x + J_{xz}^2; \\ \Gamma c_9 &= J_x; \Gamma = J_x J_z - J_{xz}^2\end{aligned}\quad (26)$$

The vehicle inertia is defined [31] as

$$\mathbf{J} = \begin{bmatrix} J_x & 0 & -J_{xz} \\ 0 & J_y & 0 \\ -J_{xz} & 0 & J_z \end{bmatrix}\quad (27)$$

Aerodynamic moments are given by [31]

$$L = Q S b \left\{ \begin{aligned} &cl_\beta \beta + cl_{\delta_n} \delta_n + cl_{\delta_l} \delta_l + cl_\Delta \Delta_n \dots \\ &\dots + \frac{b}{2v_R} (cl_p p + cl_r r) \end{aligned} \right\}\quad (28)$$

$$N = Q S b \left\{ \begin{aligned} &cn_\beta \beta + cn_{\delta_n} \delta_n + cn_{\delta_l} \delta_l + cn_\Delta \Delta_n \dots \\ &\dots + \frac{b}{2v_R} (cn_p p + cn_r r) \end{aligned} \right\}\quad (29)$$

$$M = Q S L_{ref} \left\{ cm_\alpha \alpha + cm_{\delta_m} \delta_m + \frac{L_{ref}}{v_R} cm_q q \right\}\quad (30)$$

Introducing the stability derivatives, we obtain

$$\dot{p} = L_\beta \beta + L_p p + L_r r + L_{\delta_n} \delta_n + L_{\delta_l} \delta_l \dots \dots + L_\Delta \Delta_n + (c_1 r + c_2 p)q\quad (31)$$

$$\begin{aligned}\dot{q} &= M_\alpha \alpha + M_q q + M_{\delta_m} \delta_m + c_5 p r \dots \\ &\dots - c_6 (p^2 - r^2)\end{aligned}\quad (32)$$

$$\begin{aligned}\dot{r} &= N_\beta \beta + N_p p + N_r r + N_{\delta_n} \delta_n + N_{\delta_l} \delta_l \dots \\ &\dots + N_\Delta \Delta_n + (c_8 p - c_2 r)q \\ L_{(.)} &= \frac{\partial \dot{p}}{\partial (.)}; (.) = \beta, p, r, \delta_l, \delta_n, \Delta_n; M_{(.)} = \frac{\partial \dot{q}}{\partial (.)}; \\ N_{(.)} &= \frac{\partial \dot{r}}{\partial (.)}; (.) = \beta, p, r, \delta_l, \Delta_n, \delta_n\end{aligned}\quad (33)$$

If lateral aerodynamic forces are negligible[†] and angle of attack is small, the dynamics of longitudinal velocity, angle of attack, sideslip angle, roll angle, air path bank angle and

flight path angle linearized dynamics are given by

$$\begin{aligned}\Delta \dot{v}_R &= X_v \Delta v_R + X_\alpha \Delta \alpha + X_{\delta_m} \Delta \delta_m + X_{\delta_n} \delta_n + X_{\delta_l} \delta_l - \xi_x g \\ \Delta \dot{\alpha} &= q - Z_\alpha \Delta \alpha - Z_{\delta_m} \delta_m - Z_\Delta \Delta_m + \frac{g}{v_R} (\xi_z \cos(\mu) + \xi_y \sin(\mu)) \\ \dot{\beta} &= -r + Y_\beta \beta + Y_{\delta_n} \delta_n + Y_{\delta_l} \delta_l + Y_{\Delta_n} \Delta_n + \frac{g}{v_R} (\xi_z \sin(\mu) - \xi_y \cos(\mu))\end{aligned}\quad (34)$$

$$\dot{\mu} = p + \cos(\gamma) \dot{\gamma}$$

$$\dot{\gamma} = \cos(\mu) (Z_v \Delta v_R + Z_\alpha \Delta \alpha + Z_{\delta_m} \Delta \delta_m + Z_\Delta \Delta) - \xi_z g v_R$$

with $v_R = v_0 + \Delta v_R$, $\alpha = \alpha_0 + \Delta \alpha$, $\delta_m = \delta_m^{Trim} + \Delta \delta_m$ and

$$X_{(.)} = \partial v_R / \partial (.); (.) = v_R, \alpha, \delta_m, \delta_n, \delta_l, \Delta_\alpha$$

$$Y_{(.)} = \partial \dot{\gamma} / \partial (.); (.) = \beta, r, \delta_n, \Delta_n$$

$$Z_{(.)} = \partial \dot{\gamma} / \partial (.); (.) = \alpha, q, \delta_m, \Delta_m$$

Using τ_A, τ_T as the first order time constants, the aerodynamic controls and thruster actuator dynamics are represented by

$$\tau_{aero} \dot{\delta}_{(.)} = -\delta_{(.)} + u_{(.)}, (.) = l, m, n; \quad \tau_{thrust} \dot{\Delta}_n = -\Delta_n + u_{\Delta_n}\quad (35)$$

2.2.2. Notional Vehicle

A notional hypersonic vehicle is considered to evaluate the validity of the closed form performance formulations. A clipped delta shaped glide vehicle is considered as shown in Figure 1. The aerodynamic coefficients were developed using the Hypersonic Arbitrary Body Program (HABP) code. The vehicle mass is 318 kg with a reference surface $S = 1.28 \text{ m}^2$ a reference chord of $L_{ref} = 2.52 \text{ m}$ and a span of $b = 0.78 \text{ m}$. In this work additional yaw thrusters at the front of the vehicle have been considered. Referring to Figure 1, the differential deflection of the control flaps can create a roll moment and the deflection of the yaw flap a yaw moment. Numerical values of the stability derivatives in (22-23, 27-33) are shown in Table-1.

2.2.3. Initial Conditions and Perturbations

Initial altitude = 55,000 m, Mach number = 20, initial. Initial roll angle is $\phi_0 = 1 \text{ rad}$ with initial sideslip angle $\beta_0 = -0.0175 \text{ rad}$. The fact that initial roll angle and sideslip angle are of opposite signs of course, represents an additional challenge. Initial angle of attack $\alpha_0 = 0.135 \text{ rad}$, a value half of what is required for sustaining horizontal flight with corresponding initial roll angle. The model is very uncertain, as discussed in the introductory section; therefore, in theory, uncertainties should be applied to the entire set of the coefficients of (19, 22-23) and (31-33). However, since the design of HOSM autopilot only uses the coefficients of the control terms, that is $L_{\delta_l}, M_{\delta_m}, N_{\delta_n}, N_{\Delta_n}$, therefore, from a practical point of view, disturbances need only to be included in the control terms $M_{\delta_m}, N_{\delta_n}$ of pitch and yaw rate in (36) and in (23) for Z_α, Y_β .

[†] Otherwise they are treated as unknown but bounded disturbances



Figure 1. Vehicle Considered.

Two types of perturbations are applied to the aerodynamics model:

Type 1: Sinewave type multiplicative disturbance which may be caused by elastic modes and recognizable by their tilde are applied to $M_{\delta m}, N_{\delta n}$

$$\begin{aligned}\tilde{M}_{\delta m} &= d_{\alpha} (\sin(\varpi_{\alpha} + \phi_{\alpha})) \bar{M}_{\delta m}; M_{\delta m} = \bar{M}_{\delta m} + \tilde{M}_{\delta m} \\ \tilde{N}_{\delta n} &= d_{\beta} (\sin(\varpi_{\beta} + \phi_{\beta})) \bar{N}_{\delta n}; N_{\delta n} = \bar{N}_{\delta n} + \tilde{N}_{\delta n} \\ \tilde{Z}_{\alpha} &= D_{\alpha} \bar{Z}_{\alpha}; t > t_{\alpha} \quad Z_{\alpha} = \bar{Z}_{\alpha} + \tilde{Z}_{\alpha} \\ \tilde{Y}_{\beta} &= D_{\beta} \bar{Y}_{\beta}; t > t_{\beta} \quad Y_{\beta} = \bar{Y}_{\beta} + \tilde{Y}_{\beta}\end{aligned}\quad (36)$$

Type 2: Step like multiplicative disturbances are applied to Z_{α}, Y_{β} which may be caused by sudden separation of pieces of thermal protection which would create locally a shock wave thereby modifying the air flow in a step wise fashion.

$$\begin{aligned}\tilde{Z}_{\alpha} &= D_{\alpha} \bar{Z}_{\alpha}; t > t_{\alpha} \quad Z_{\alpha} = \bar{Z}_{\alpha} + \tilde{Z}_{\alpha} \\ \tilde{Y}_{\beta} &= D_{\beta} \bar{Y}_{\beta}; t > t_{\beta} \quad Y_{\beta} = \bar{Y}_{\beta} + \tilde{Y}_{\beta}\end{aligned}\quad (37)$$

where $D_{\alpha}, D_{\beta}, d_{\alpha}, d_{\beta}, \varpi_{\alpha}, \varpi_{\beta}, \phi_{\alpha}, \phi_{\beta}$ are random uniformly distributed disturbance terms assumed to remain constant during the flight scenario.

Also, it is assumed that

(A3): The autopilot generates prescribed normal and transversal trajectories.

(A4): The commanded angle of attack, roll and sideslip angles the autopilot uses as pseudo controls.

(A5): Angle of attack and roll angle command trajectories are shaped by a second order filter to produce two pairs, $\alpha^*, \dot{\alpha}^*$ and $\phi^*, \dot{\phi}^*$ which are the inputs to the autopilot. The flying quality filters that generate smooth commands are defined as

$$\begin{aligned}\ddot{\phi}^* &= -\omega_{\phi}^2 \phi^* - 2\omega_{\phi} \dot{\phi}^* + \omega_{\phi}^2 \phi_c; \quad \omega_{\phi} = 3 \\ \ddot{\alpha}^* &= -\omega_{\alpha}^2 \alpha^* - 2\omega_{\alpha} \dot{\alpha}^* + \omega_{\alpha}^2 \alpha_c; \quad \omega_{\alpha} = 5\end{aligned}\quad (38)$$

2.2.4. Problem Formulation

Given the prescribed angle of attack and roll angle trajectories $\alpha(t)^*, \phi(t)^*$ calculated by the inversion of guidance commands and filtered in accordance with (38), the normal and lateral commanded acceleration autopilot design problem is formulated in a two-fold format:

Task 1: Design Adaptive HOSM aerodynamic angle controller for the hypersonic glider (19-35) in terms of

u_m, u_l, u_n that generates pitch, roll and yaw actuator commands u_m, u_l, u_n such that

$$e_{\alpha}, \dot{e}_{\alpha}, e_{\phi}, \dot{e}_{\phi}, e_{\beta}, \dot{e}_{\beta} \rightarrow 0 \quad (39)$$

as time increases in the presence of bounded additive and multiplicative perturbations defined by (36-37), where

$$e_{\alpha} = \alpha(t)^* - \alpha, \quad e_{\phi} = \phi(t)^* - \phi, \quad e_{\beta} = \beta(t)^* - \beta, \quad \beta(t)^* = 0$$

Task 2:-Design the impulsive part of the sideslip angle controller for the hypersonic glider (19-35) in term of $u_{\Delta n}$ that is to be employed in exceptional circumstances when the sideslip angle transient value exceeds some critical threshold, $|\beta| > \beta_{\max}$, in order to drive $\beta \rightarrow 0, \dot{\beta} \rightarrow 0$ in a short time, i.e. < 0.4 sec.

Remark 7: The control functions u_m, u_l, u_n and $u_{\Delta n}$ are designed in terms of $\delta_m, \delta_l, \delta_n$, and Δ_n while neglecting the dynamics of the actuators (35), which are considered as unmodeled dynamics and as such, not considered in the design while their effects are modeled in the simulations.

2.3. Nonlinear Dynamic Sliding Manifold HOSM Controller Designs

2.3.1. Sliding Variable Dynamics

Nonlinear, HOSM Dynamic Sliding Manifold (NDSM) controllers [27] are designed in this section to provide a basis of comparison with the new proposed designs. Actuator dynamics in (35) are neglected in the controller design; however, their dynamics are introduced in the simulations. Likewise, lift and transverse lift created by the actuators, while neglected in the controller design by nullifying their effects as $Z_{\delta m} \delta_m = Y_{\delta n} \delta_n \approx 0$, are included in the simulation.

Equation (39) is enforced in the sliding mode by introducing the sliding variables

$$\begin{aligned}\sigma_{\phi} &= \varpi_{\phi} \int (\phi^* - \phi) d\tau + (\phi^* - \phi); \quad \varpi_{\phi} = 5 \\ \sigma_{\alpha} &= \varpi_{\alpha} \int (\alpha^* - \alpha) d\tau + (\alpha^* - \alpha); \quad \varpi_{\alpha} = 10 \\ \sigma_{\beta} &= \varpi_{\beta} \int \beta d\tau + \beta; \quad \varpi_{\beta} = 5\end{aligned}\quad (40)$$

that are to be driven to zero in finite time by the continuous fixed-gain and adaptive-gain HOSM controllers. Apparently, (39) hold as soon as the sliding variables $\sigma_{\alpha}, \sigma_{\phi}, \sigma_{\beta} \rightarrow 0$ in finite time.

Remark 8: Here while continuous control algorithms are used their digital implementation at 10 KHz may result in some small biases. The proportional integral format of the sliding variables in (40) is chosen to mitigate possible constant biases in the tracking errors $e_{\alpha}, e_{\phi}, e_{\beta}$.

Again, the dynamics of the actuators in (35) are neglected while deriving the sliding variables' input-output dynamics. Using (24-34) and (40), second order input-output dynamics of the roll sliding variable σ_{ϕ} are derived as

$$\ddot{\sigma}_\phi = f_\phi - (\bar{L}_{\delta l} + \tilde{L}_{\delta l})\delta_l \quad (41)$$

with

$$f_\phi = -\frac{d}{dt} [q \sin(\phi) \tan(\theta) + r \cos(\phi) \tan(\theta)] - L_\beta \beta - L_p p - L_r r - L_{\delta n} \delta_n - L_\Delta \Delta_n - (c_1 r + c_2 p)q + \bar{\omega}_\phi \dot{\phi}^* + \ddot{\phi}^* - \bar{\omega}_\phi \dot{\phi} \quad (42)$$

where, it is assumed that $\frac{|\tilde{L}_{\delta l}|}{|\bar{L}_{\delta l}|} = \bar{\epsilon}_{\delta l}$, $0 \leq \bar{\epsilon}_{\delta l} < 1$ and thus, (41) becomes

$$\ddot{\sigma}_\phi = \underbrace{f_\phi - \tilde{L}_{\delta l} \delta_l}_{\tilde{f}_\phi} - \bar{L}_{\delta l} \delta_l \quad (43)$$

where \tilde{f}_ϕ is an unknown bounded perturbation. Using (24-34) and (40) the input-output dynamics of the sliding variable σ_α for the angle of attack are derived as

$$\ddot{\sigma}_\alpha = f_\alpha - (\bar{M}_{\delta m} + \tilde{M}_{\delta m})\delta_m \quad (44)$$

with

$$f_\alpha = \frac{d}{dt} \left[\frac{g}{v_R} \langle \cos(\mu) \xi_z + \sin(\mu) \xi_y \rangle - Z_\alpha \alpha - Z_{\delta m} \delta_m \right] - M_\alpha \alpha + M_q q + c_5 p r - c_6 (p^2 - r^2) + \bar{\omega}_\alpha \dot{\alpha}^* + \ddot{\alpha}^* - \bar{\omega}_\alpha \dot{\alpha} \quad (45)$$

where it is assumed that $\frac{|\tilde{M}_{\delta m}|}{|\bar{M}_{\delta m}|} = \bar{\epsilon}_{\delta m}$, $0 \leq \bar{\epsilon}_{\delta m} < 1$ and thus, (44) becomes

$$\ddot{\sigma}_\alpha = \underbrace{f_\alpha - \tilde{M}_{\delta m} \delta_m}_{\tilde{f}_\alpha} - \bar{M}_{\delta m} \delta_m \quad (46)$$

where \tilde{f}_α is an unknown bounded perturbation. Using (20-24) and (40) the input-output dynamics of the sliding variable σ_β for the sideslip angle are derived as

$$\ddot{\sigma}_\beta = f_\beta + (\bar{N}_{\delta n} + \tilde{N}_{\delta n})\delta_n \quad (47)$$

with

$$f_\beta = \frac{d}{dt} \left[-Y_\beta \beta - Y_{\delta n} \delta_n - Y_{\delta l} \delta_l - Y_{\Delta n} \Delta_n \dots \right] + N_\beta \beta + N_p p + N_r r + N_{\delta l} \delta_l + N_\Delta \Delta_n + (c_8 p - c_2 r)q - \bar{\omega}_\beta \dot{\beta} \quad (48)$$

where it is assumed that $\frac{|\tilde{N}_{\delta n}|}{|\bar{N}_{\delta n}|} = \bar{\epsilon}_{\delta n}$, $0 \leq \bar{\epsilon}_{\delta n} < 1$ and thus, (47) becomes

$$\ddot{\sigma}_\beta = \underbrace{f_\beta + \tilde{M}_{\delta n} \delta_n}_{\tilde{f}_\beta} + \bar{N}_{\delta n} \delta_n \quad (49)$$

where \tilde{f}_β is an unknown bounded perturbation.

Remark 9: The design of the continuous second order sliding mode controllers (2-SMC, a case of HOSM controller) that drives $\sigma_\alpha, \sigma_\phi, \sigma_\beta \rightarrow 0$ in finite time is presented in Sub-sections 2.4 and 2.5.

2.3.2. Second Order Sliding Mode Control Based on Nonlinear Dynamic Sliding Manifold

The Non Linear Dynamic Sliding Manifold (NDSM) based controller [5, 31] that does not require differentiating the sliding variables $\sigma_\phi, \sigma_\alpha, \sigma_\beta$, is used for (43), (46), and (49) of relative degree 2 to drive $\sigma_\phi, \dot{\sigma}_\phi \rightarrow 0$, $\sigma_\alpha, \dot{\sigma}_\alpha \rightarrow 0$, and $\sigma_\beta, \dot{\sigma}_\beta \rightarrow 0$ in finite time in the presence of the bounded perturbations. This is

$$\begin{aligned} \dot{\chi}_{(.)} &= \eta_{2(.)} |\sigma_{(.)}|^{1/2} \text{sign}(\sigma_{(.)}) - \eta_{1(.)} |\chi_{(.)}|^{1/2} \text{sign}(\chi_{(.)}); \\ u_{(.)} &= \eta_{3(.)} \cdot \text{sign}(\sigma_{(.)} + \chi_{(.)}) + u_{Trim}; \quad (.) = \phi, \alpha, \beta \end{aligned} \quad (50)$$

where $u_{Trim} = (-M_\alpha \alpha - M_q q_{curv}) / M_{\delta m}$ applies only to the control of the angle of attack with the term q_{curv} being approximately computed as $q_{curv} = -v_R / (r_\oplus + h)$.

Note that the design parameters $\eta_{1(.)}, \eta_{2(.)}, \eta_{3(.)} > 0$ are to be tuned so that $\sigma_\phi, \sigma_\alpha, \sigma_\beta$ and their derivatives converge to zero in finite time. Specifically, $\eta_{3(.)}$ that is responsible for convergence to the NDSM $J_{(.)} = \sigma_{(.)} + \chi_{(.)} = 0$ is to exceed the boundary of the corresponding disturbance divided by the minimal value of the control gain; $\eta_{2(.)}$ is to be selected based on the desired convergence time $\sigma_{(.)}, \dot{\sigma}_{(.)} \rightarrow 0$ as soon as the NDSM $J_{(.)} = \sigma_{(.)} + \chi_{(.)} = 0$ is reached and hold, and $\eta_{1(.)} > 0$.

Remark 10: To achieve continuity of control $u_{(.)} = l, m, n$ the “sign” in (50) may be approximated by saturation “sat” function, i.e. $\text{sign}(\sigma_{(.)} + \chi_{(.)}) \rightarrow \text{sat}_{\epsilon_0}(\sigma_{(.)} + \chi_{(.)})$ where $\epsilon_0 > 0$ is a small width of a linearity zone.

2.4. Continuous Fixed-gain HOSM Controller Design

It is assumed herein, that the derivatives of the disturbances in (43, 47, 49) are bounded: $|\dot{\tilde{f}}_{(.)}| < H_{(.)}$ and that $H_{(.)} > 0$ terms are known. In accordance with Theorem 2, the Hurwitz second order polynomials ($r = 2$) $s^2 + \gamma_{2(.)} s + \gamma_{1(.)}$; $(.) = \phi, \alpha, \beta$ are defined with exponents $a_{1(.)}, a_{2(.)}$ being calculated accordingly as in (3)

$$\begin{aligned} a_{1(i)} &= a_{2(i)} / (2 - a_{2(i)}); \quad a_{2(i)} = a_{(i)}; \\ a_{(i)} &\in (1 - \varepsilon, 1); \quad \varepsilon \in (0, 1) \end{aligned} \quad (51)$$

where

$$\begin{aligned} \gamma_{1\phi} &= 100; \quad \gamma_{2\phi} = 20; \quad a_{\phi} = 0.6 \\ \gamma_{1\alpha} &= 400; \quad \gamma_{2\alpha} = 40; \quad a_{\alpha} = 0.8 \\ \gamma_{1\beta} &= 100; \quad \gamma_{2\beta} = 20; \quad a_{\beta} = 0.8 \end{aligned} \quad (52)$$

Therefore, HOSM fixed-gain controllers are designed as

$$\begin{aligned} u_{[i]} &= -\gamma_{2(i)} |\dot{\sigma}_{(i)}|^{a_{2(i)}} \text{sign}(\dot{\sigma}_{(i)}) - \gamma_{1(i)} |\sigma_{(i)}|^{a_{1(i)}} \text{sign}(\sigma_{(i)}) - \lambda_{(i)}; \\ (.) &= \phi, \alpha, \beta; \quad [i] = l, m, n \end{aligned} \quad (53)$$

$$\begin{aligned} s_{(i)} &= \dot{\sigma}_{(i)} + z_{(i)}; \quad \dot{z}_{(i)} = u_{[i]} - \lambda_{(i)}; \quad (.) = \phi, \alpha, \beta \\ \dot{\lambda}_{(i)} &= \eta_{4(i)} |s_{(i)}|^{1/2} \text{sign}(s_{(i)}) + \xi_{(i)}; \quad [i] = l, m, n \\ \dot{\xi}_{(i)} &= \eta_{5(i)} \text{sign}(s_{(i)}) \end{aligned} \quad (54)$$

where $\eta_{4(i)} = 1.1 |H_{(i)}|$; $\eta_{5(i)} = 1.5 |H_{(i)}|^{1/2}$.

In accordance with Theorem 2, the continuous HOSM controllers in (53-54) drive $\sigma_{\alpha}, \sigma_{\phi}, \sigma_{\beta} \rightarrow 0$ in finite time provided that the disturbances $\bar{f}_{(i)}$ have bounded derivatives.

Remark 11: The dynamics of the actuators are included in the simulation.

2.5. Continuous Adaptive HOSM Controller Design

In accordance with Theorems 2 and 3 the structure of the Continuous Adaptive HOSM control is the same as of the continuous fixed-gain HOSM control. The difference resides in the design of the injection term $\lambda_{(i)}$. In this case it is assumed that the boundaries of the first two derivatives of the disturbances $|\dot{f}_{(i)}(t)| \leq H_{(i)}$, and $|\ddot{f}_{(i)}(t)| \leq N_{(i)}$, $N_{(i)} > 0$, $H_{(i)} > 0$ exist but are unknown. The adaptation of injection term $\lambda_{(i)}$ aimed at reconstructing the disturbances thus becomes inevitable for preventing the overestimation of the gains and associated chattering caused by un-modeled dynamics [11, 16].

The adaptive Super-Twisting injection term $\lambda_{(i)}$ is designed in accordance with Theorem 3 and (8) as

$$\begin{aligned} \lambda_{(i)} &= \eta_{3(i)} |s_{(i)}|^{1/2} \text{sign}(s_{(i)}) + w_{(i)} \\ \dot{w}_{(i)} &= k_{(i)}(t) \text{sign}(s_{(i)}) \end{aligned} \quad (55)$$

where $\eta_{3(i)} > 0$ are selected large enough and the adaptive gains $k_{(i)}(t)$ are selected in accordance with the double-layer adaptation algorithm presented in Theorem 3 by (9-12)

$$\begin{aligned} \dot{k}_{(i)}(t) &= -(\rho_{0(i)} + \rho_{(i)}(t)) \text{sign}(v_{(i)}(t)) \\ \dot{\rho}_{(i)}(t) &= \bar{\gamma}_{(i)} |v_{(i)}(t)| \\ v_{(i)}(t) &= k_{(i)}(t) - |\hat{w}_{eq(i)}(t)| / \varepsilon_{1(i)} - \varepsilon_{2(i)} \end{aligned} \quad (56)$$

The parameters in (56) are selected with $\rho_{0(i)} > 0$, $\bar{\gamma}_{(i)} > 0$, $\varepsilon_{1(i)} \in (0, 1)$, and $\varepsilon_{2(i)} > 0$ are small numbers.

The equivalent control $w_{eq(i)}(t)$ is estimated by $\hat{w}_{eq(i)}(t)$ via low pass filtering which removes higher frequency components of the control $w_{(i)}(t)$ in (55)

$$\hat{w}_{eq(i)}(t) = \text{Low Pass Filtering}(w_{(i)}(t)) \quad (57)$$

2.6. Impulsive Sideslip Angle Control

The impulsive control is designed based in accordance with Theorem 4 and (15-16) and is applied to drive the sideslip angle to the origin in a short time. The following additional assumptions were made:

(A6): No aerodynamic yaw control is applied during the application of successive yaw impulses.

(A7): Yaw and roll dampening terms are small and thus, can be neglected.

(A8): Small inertial acceleration terms are deemed to be negligible.

(A9): Terms proportional to δ_i and $\dot{\Delta}_n$ are also negligible.

(A10): Thruster dynamics is not considered in the design but is modeled in the simulation.

The sideslip dynamics is given by (23-24) and its input-output dynamics are presented as

$$\begin{aligned} \ddot{\beta} &= Y_{\beta} \dot{\beta} - N_{\beta} \beta - N_{\Delta n} \Delta_n + \Psi_n \\ \Psi_n &= \frac{d}{dt} \left[Y_{\delta n} \delta_n + Y_{\delta l} \delta_l + \frac{g}{v_R} \langle \cos(\mu) \xi_y - \sin(\mu) \xi_z \rangle \right] \dots \\ &\quad - \{ N_p p + N_r r + N_{\delta n} \delta_n + N_{\delta l} \delta_l + (c_8 p - c_2 r) q \} + Y_{\Delta n} \dot{\Delta}_n \end{aligned} \quad (58)$$

where Ψ_n represents a small unknown perturbation.

The effects caused by the term Ψ_n in (59) precludes achieving a perfectly exact dead-beat in (15, 17) control that drives $\beta \rightarrow 0$ and $\dot{\beta} \rightarrow 0$ in a timely fashion. This is not a source of concern since the purpose of this impulsive control is only to reduce sufficiently the magnitude of $\beta, \dot{\beta}$ in a short time interval $h_{\Delta} < 0.4$ sec. It is followed thereafter by the application of a continuous HOSM control that provides desired convergence accuracy and robustness. We can note inclusion of the impulse $\dot{\Delta}_n$ as part of the disturbance Ψ_n .

Equation (58) is given in a state variable format which excludes Ψ_n as

$$\frac{d}{dt} \begin{bmatrix} \beta \\ \dot{\beta} \end{bmatrix} = \begin{bmatrix} 0 & 1 \\ -N_\beta & Y_\beta \end{bmatrix} \begin{bmatrix} \beta \\ \dot{\beta} \end{bmatrix} + \begin{bmatrix} 0 \\ -N_{\Delta n} \end{bmatrix} \Delta_n \quad (59)$$

Given an initial state at t_f : $\mathbf{X}(t_f) = [\beta(t_f) \ \dot{\beta}(t_f)]^T$, a sequence of impulses is to be generated such that $\mathbf{X}(t_f + h_\Delta) \rightarrow [0 \ 0]^T$. The solution of this problem is the control law $u_{\Delta n}(t)$:

$$\begin{bmatrix} \beta(t_f) \\ \dot{\beta}(t_f) \end{bmatrix} = \int_{t_f}^{t_f + h_\Delta} \exp(-\mathbf{A}\tau) \mathbf{B} u_{\Delta n}(\tau) d\tau \quad (60)$$

The impulsive control [19-24] that drives $\beta, \dot{\beta} \rightarrow \approx 0$ by time $t = h_\Delta$ is defined in accordance with (15-16) as

$$u_{\Delta n} = \sum_{k=0}^{r-1} \alpha_k \delta_\varepsilon^{(k)}(t) \quad (61)$$

Where $\delta_\varepsilon^{(k)}$ are the generalized derivatives of the Dirac delta-function centered in $\varepsilon > 0$ defined in [25]. Corresponding piecewise-constant function approximations for $\delta_\varepsilon^{(0)}(t), \delta_\varepsilon^{(1)}(t)$ are defined as in [24]

$$\hat{\delta}_{h_\Delta}(t) = \begin{cases} 1/h_\Delta; & \text{if } 0 \leq t \leq h_\Delta \\ 0 & \text{otherwise} \end{cases}, \quad (62)$$

$$\hat{\delta}_{h_\Delta}^{(1)}(t) = \begin{cases} 4/h_\Delta^2; & \text{if } 0 \leq t \leq h_\Delta/2 \\ -4/h_\Delta^2; & \text{if } h_\Delta/2 \leq t \leq h_\Delta \\ 0; & \text{otherwise} \end{cases}$$

Given that the impulse is short it is reasonable to expand $\exp(-\mathbf{A}\tau)$ as, as

$$\exp(-\mathbf{A}\tau) = \begin{bmatrix} 1 & -\tau \\ -N_\beta \tau & 1 - \tau Y_\beta \end{bmatrix}; \quad \mathbf{A} = \begin{bmatrix} 0 & 1 \\ -N_\beta & Y_\beta \end{bmatrix} \quad (63)$$

and

$$\exp(-\mathbf{A}\tau) \mathbf{B} = \begin{bmatrix} -\tau \\ 1 - \tau Y_\beta \end{bmatrix} N_{\Delta n}; \quad \mathbf{B} = \begin{bmatrix} 0 \\ -N_{\Delta n} \end{bmatrix} \quad (64)$$

The first component of the vector (60) is defined as

$$\beta(t_f) = -N_{\Delta n} \left(\alpha_0 \int_0^{h_\Delta} \frac{\tau}{h_\Delta} d\tau + \alpha_1 \int_0^{h_\Delta/2} \frac{4\tau}{h_\Delta^2} d\tau - \alpha_1 \int_{h_\Delta/2}^{h_\Delta} \frac{4\tau}{h_\Delta^2} d\tau \right) \quad (65)$$

That is,

$$\beta(t_f) = N_{\Delta n} (-\alpha_0 h_\Delta / 2 + \alpha_1) \quad (66)$$

The second term of vector (60) is defined as

$$\dot{\beta}(t_f) = Y_{\Delta n} N_{\Delta n} (\alpha_0 - Y_\beta \alpha_0 \frac{h_\Delta}{2} + \alpha_1 Y_\beta) + \dots N_{\Delta n} \left(\int_0^{h_\Delta} \frac{\alpha_0}{h_\Delta} d\tau + \int_0^{h_\Delta/2} \frac{\alpha_1}{h_\Delta^2} \tau d\tau - \int_{h_\Delta/2}^{h_\Delta} \frac{\alpha_1}{h_\Delta^2} \tau d\tau \right) \quad (67)$$

Next, we obtain

$$\dot{\beta}(t_f) = N_{\Delta n} (\alpha_0 - Y_\beta \alpha_0 \frac{h_\Delta}{2} + \alpha_1 Y_\beta) \quad (68)$$

The inversion of (66, 67) yields

$$\begin{pmatrix} \alpha_0 \\ \alpha_1 \end{pmatrix} = \frac{1}{N_{\Delta n}} \begin{pmatrix} -Y_\beta \beta(h_\Delta) + \dot{\beta}(h_\Delta) \\ (1 - Y_\beta h_\Delta / 2) \beta(h_\Delta) + h_\Delta \dot{\beta}(h_\Delta) \end{pmatrix} \quad (69)$$

Finally, the impulsive control (61), designed in terms of generalized Dirac impulses as in (62) becomes

$$u_{\Delta n} = \frac{1}{N_{\Delta n}} \left(\alpha_0 \hat{\delta}_{h_\Delta}(t) + \alpha_1 \hat{\delta}_{h_\Delta}^{(1)}(t) \right) \quad (70)$$

3. Results

3.1. Simulation Approach

The quest for high Lift-to-Drag ratios leads designers to reduce as much as possible non-lifting parts of the vehicle. This requires, reducing and eliminating if possible tail surfaces and eventually resorting to flying wings. Such aerodynamic shapes do not exhibit much natural transverse stability and only provide limited control authority. It is, therefore, imperative to avoid situations where sideslip angle values exceed maximum control authority. The approach investigated in this work is an impulsive lateral control for driving to a quasi-null value the sideslip angle in a timely fashion, whenever eventually its value may exceed some maximum critical value. This impulsive control is powered by on-off thrusters and is supposed to be only used a few times during the flight, when such exceptional circumstances require it.

Four control designs were simulated; the first one, based on finite convergence time continuous NDSM-based 2-SMC controller, the second controller represents an implementation of the fixed-gain continuous HOSM control algorithm; the third controller is the implementation of the adaptive-gain HOSM algorithm; and the fourth one is a hybrid continuous adaptive-gain HOSM – impulsive controller. The results of the first design are used as reference cases for comparison with the other advanced designs. The robustness of studied continuous HOSM controllers and the hybrid continuous HOSM-impulsive controller is evaluated for time varying sinewave and step perturbations of the pitch and yaw models. Whereas no direct perturbations were introduced in roll model, roll motion was nonetheless indirectly perturbed by the coupling with the yaw motion as shown by (31-33).

Table 1. Numerical Values.

$X_v = -5.610^{-4}$	$X_\alpha = -7.6$	$X_{\delta m} = -18.65$	$X_{\delta n} = -3.83$
$X_{\delta l} = -4.59$	$Y_\beta = -810^{-4}$	$Y_{\delta n} = -1.310^{-3}$	$Y_{\delta n} = 1.310^{-3}$
$Z_\alpha = 310^{-3}$	$Z_{\delta m} = -6.310^{-3}$	$L_\beta = -810^{-4}$	$L_{\delta l} = 118$
$L_{\delta n} = 0$	$N_\beta = 1.17$	$N_{\delta l} = 1.6$	$N_{\delta n} = 39.3$
$N_{\delta n} = 20.05$	$M_\alpha = -12.7$	$M_{\delta m} = 64$	$\tau_\alpha = 0.005$
$\tau_\Delta = 0.005$	$d_\alpha \in [-0.05..0.05]$	$d_\beta \in [-0.05..0.05]$	$D_\alpha \in [-0.1..0.1]$
$D_\beta \in [-0.1..0.1]$	$\varphi_\alpha \in [0..2\pi]$	$\varphi_\beta \in [0..2\pi]$	$\varpi_\alpha, \varpi_\beta \in [5-10]$

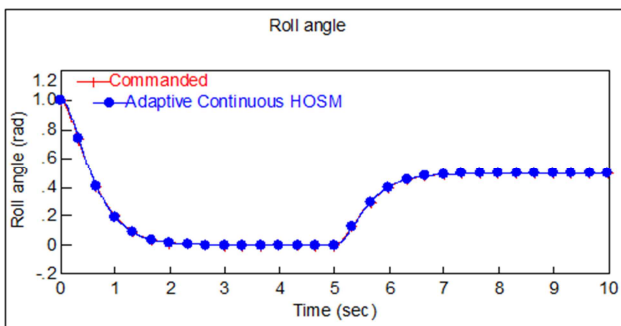
3.2. Simulation Set-Up

The model was simulated with RK-2 algorithm and 10^{-4} integration step. Table 1 shows numerical values of the model in (19-35). Corresponding values are not related to any known or planned system, nor are they supposed to represent the state of the art. The values inserted in the brackets represent the range of uniformly distributed random variables.

3.3. Roll Control

The autopilot generates reference roll angle, roll rate, angle of attack and angle of attack rate as defined by (38). It is evident that the performances of the designs considered could hardly be compared using a full-scale plot. For that matter, Figure 2 only shows commanded roll maneuver and just one of the actual responses; of the Adaptive Continuous HOSM design. Other responses are not shown because given the plot scale, they would hardly be distinguishable from the roll command.

Comparative performances of several designs considered herein are evaluated by comparing the errors of actual trajectories versus reference trajectories and by time-zooming during initial transient motions as shown by Figures 3-4.

**Figure 2.** Roll Command and Continuous Adaptive HOSM response.

Commanded and actual roll angles are represented in Figure 2 in red and blue respectively; actual trajectory follows so well commanded maneuver that their traces in Figure 4 are perfectly superimposed. The distinctive markers show that these are indeed, two traces.

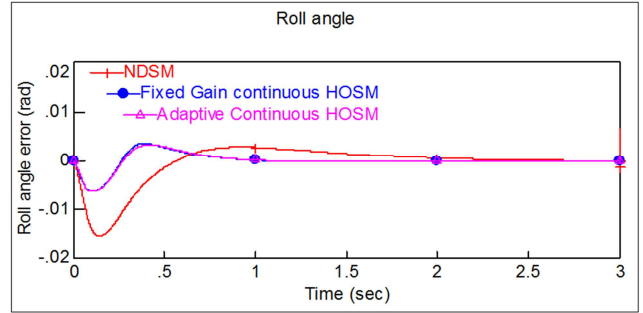
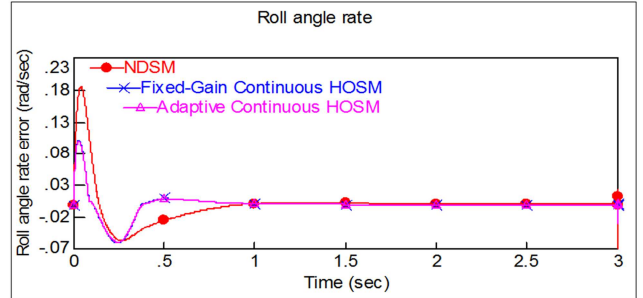
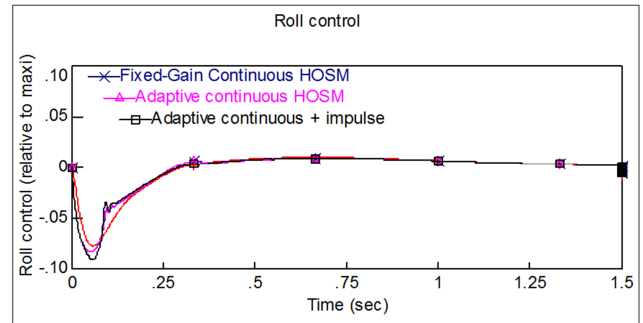
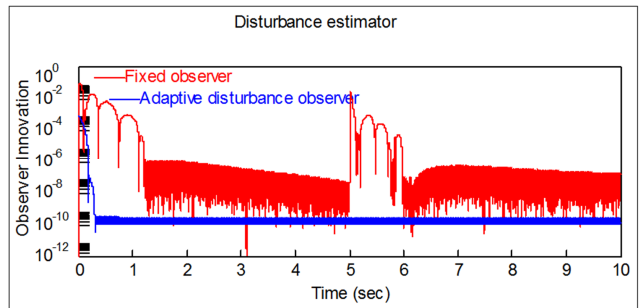
**Figure 3.** Roll Angle error response (zoomed).**Figure 4.** Roll Angle rate error response (zoomed).**Figure 5.** Roll Control.

Figure 5 represents roll for the cases of HOSM constant gain, adaptive-gain HOSM and in the presence of a yaw impulsive control. Figures 6 and 7 represent respectively roll observer's innovation and estimated value of the disturbance.

**Figure 6.** Roll Observer Innovation.

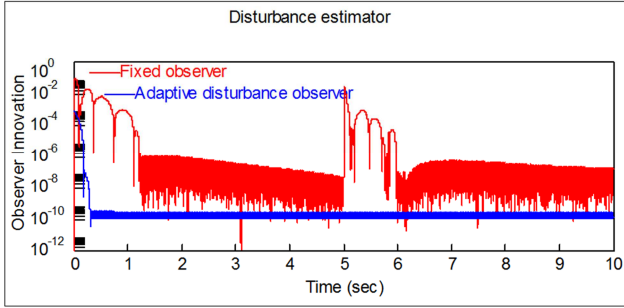


Figure 7. Estimation of roll disturbance.

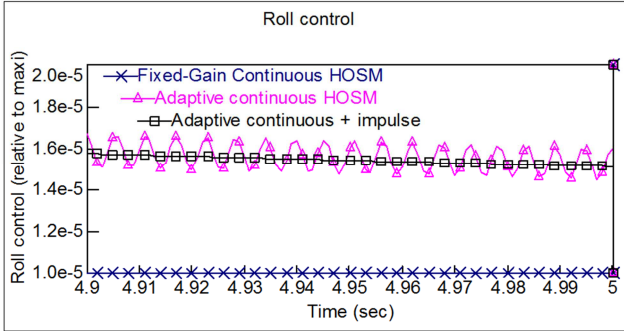


Figure 8. Roll Control (zoomed).

Remark 10: Estimated value of the (sinusoidal) injection term in Figures 5, 8 is relative to maximum control rolling moment $L_{sl} = 123 \text{ rad/sec}$; it represents, physically, rolling moment chattering amplitude about 0.01 deg/sec .

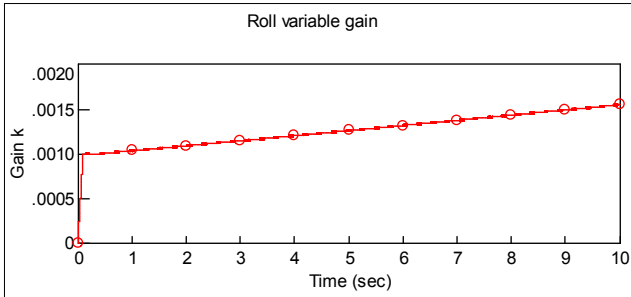


Figure 9. Adaptive gain.

Figure 9 shows the rapid variation of the gain which is coincident with the rapid convergence of the innovation in Figure 6 and then, a slow augmentation of the gain which is correlated with the slow augmentation of the value of the estimated rolling disturbance.

3.4. Sideslip Angle Control

The performance using the Continuous Adaptive HOSM control is compared with the baseline NDSM design, and the benefits of additional impulse control are evaluated. Figs. 10-11 shows that after a transient of approximately 1second, NDSM design settles the sideslip angle to a quasi-null value.

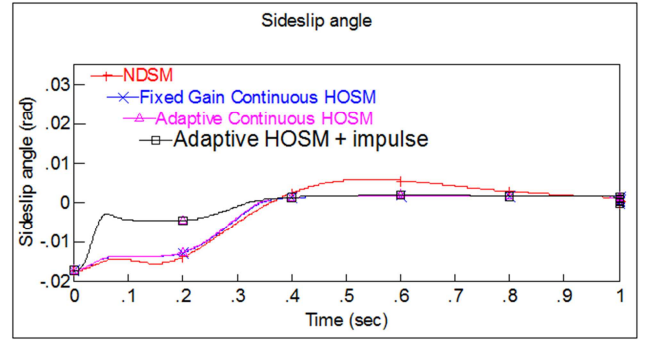


Figure 10. Sideslip Angle (zoomed).

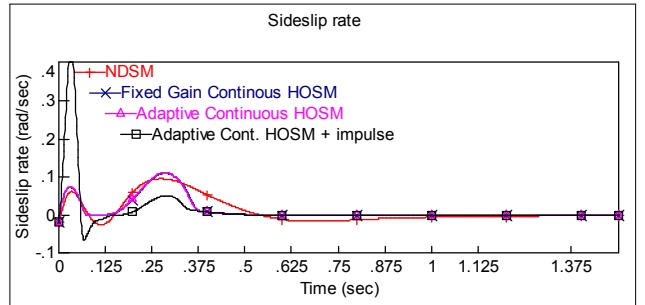
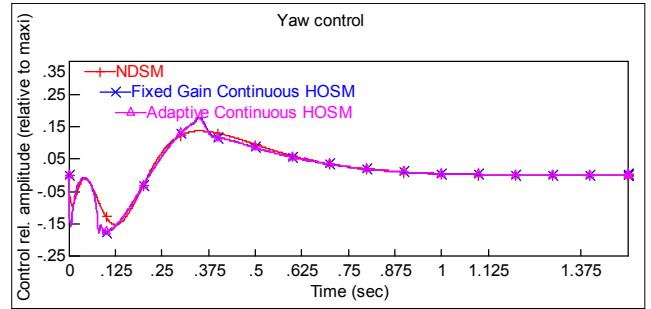
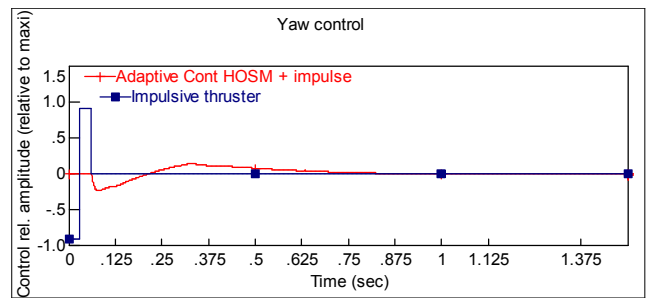


Figure 11. Sideslip rate (zoomed).



a



b

Figure 12. a. Sideslip Angle Control (w/o) impulsive control. b. Sideslip Angle Control with impulsive control.

3.5. Angle of Attack Control

The same approach is used to display the angle of attack performance. Figure 13 shows the command and the response of Continuous Adaptive HOSM. The responses of other designs are not represented in Figure 13 because they would be practically indistinguishable from the response of Continuous Adaptive HOSM design

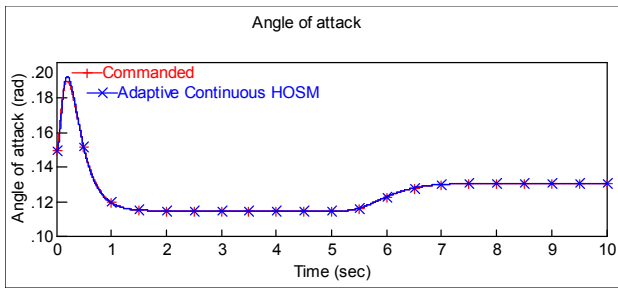


Figure 13. Angle of Attack command and Continuous Adaptive HOSM response.

The performances of the designs are evaluated shown in Figs. 14-15 by comparing corresponding error responses on a zoomed short time interval beginning at the inception of the simulation.

Since the angle of attack command is initiated at a value $a^* = 0.015 \text{ rad}$ far smaller from the required value $a^* = 0.0135 / \cos(1) = 0.027 \text{ rad}$, angle of attack rate response exhibits a small lag as shown by Figure 14; once initial error is corrected, commanded angle of attack is perfectly tracked thereafter.

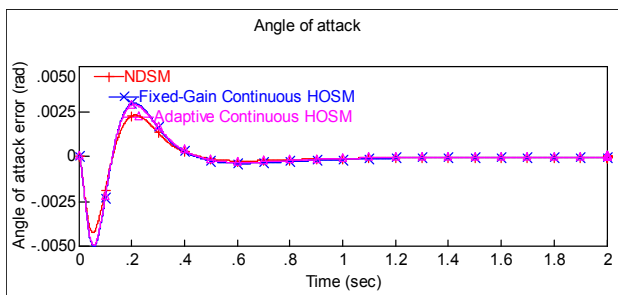


Figure 14. Angle of Attack error (zoomed).

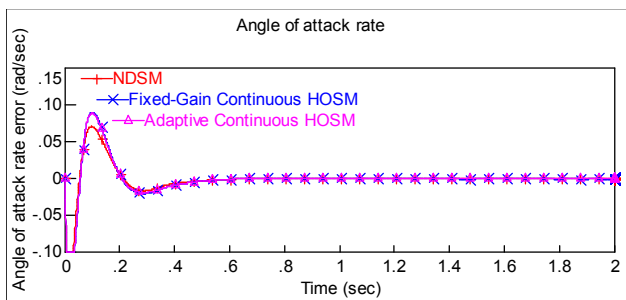


Figure 15. Angle of attack rate (zoomed).

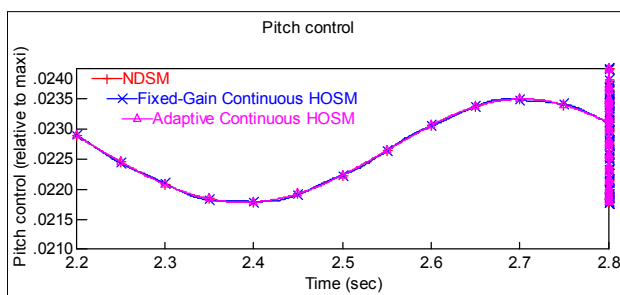


Figure 16. Pitch control (zoomed).

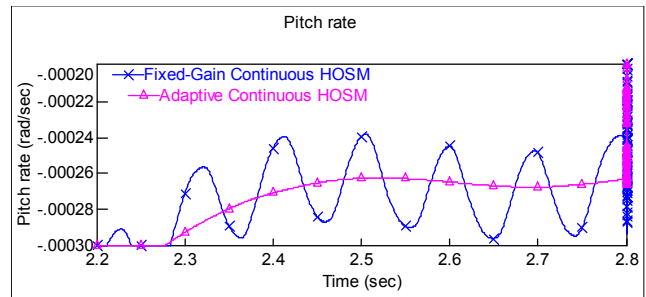


Figure 17. Pitch rate (zoomed).

Figure 16 represent the pitch control (that controls the angle of attack) and Figure 17 represents the pitch rate.

4. Discussion

4.1. Roll Control

Figures 3-4 represent respectively roll angle and roll rate error responses of NDSM vs. Continuous fixed gain and Adaptive HOSM designs. Not surprisingly the traces of Fixed Gain Continuous HOSM and Adaptive Continuous are also perfectly superimposed because the main difference is the adaptive management of the controller aimed at practically eliminating the chatter, but their equivalent controls are practically the same.

The continuous HOSM controllers achieve better performances rather than the reference results obtained with the NDSM controller as they settle in 0.5 sec. compared with 1 sec. for the NDSM.

The fact that Continuous HOSM designs, whether with fixed observers or adaptive observers, achieve comparable results that is not surprising since their equivalent controls are comparable as stated in Sub-sections 2.4 and 2.5 and only differ due to the adaptive sliding mode observer that eliminates the control chattering. This chatter is prevailing in the fixed gain observer due to the larger gain of the fixed parameter observer. Figures 6-7 show that the adaptive gain injection term in the disturbance observer (estimator) allows a much shorter observer settling time and a significantly reduced level of noise caused oscillations. The results show that although the fixed parameter innovation drops down to a 10^{-7} level by time = 1.2 second it re-augments by time = 5 second because of the mid-scenario commanded roll maneuver shown in Figure 2. This is not the case with the adaptive sliding mode observer which drives, in a timely fashion, the level of residual innovation literally to zero and keeps it thereafter.

Figure 8 shows that the fixed gain observer HOSM control exhibits a residual level of chattering with amplitude relative to maximum $\Delta u_0 = 1.2 \cdot 10^{-6}$ and that the control chattering is removed completely by the adaptive-gain observer.

4.2. Sideslip Angle Control

Continuous HOSM does not exhibit the overshoot of NDSM on the time interval [0.4, 1.0] s since it settles in 0.4 s. When

applied, impulse control reduces the magnitude of residual sideslip angle to 0.005 rad. in less than 0.1s. Similar observations can be made on the sideslip angle rate in Figure 11.

Figure 12-b shows that impulse control consists of large and brief yaw control spikes created by the firing of the yaw impulse thruster as two opposite pulses of short approximately 50 msec. duration. Corresponding plot represents actual normalized thrust (i.e. actuator response); while the command is rectangular, and actuator response reveals the effect of the characteristic frequency of the thruster dynamic response. Figure 12-a, reveals that the aerodynamic control only begins at the end of the impulse.

4.3. Angle of Attack Control

Results in Figures 13 - 15 show that the rapid transient of the correction of initial errors is followed by quasi-null errors. Commanded angle of attack is modified to account for the term $1/\cos(\phi^*)$ as initial commanded roll angle at the beginning of the scenario is equal to one radian, while a second roll maneuver is undertaken on the time interval [5, 7] s.

4.4. Cancellation of Disturbances

Using (36), the amplitude of the pitch rate disturbance is given by

$$\Delta \dot{q} = \tilde{M}_{\delta m} \delta_m; \quad \tilde{M}_{\delta m} = d_\alpha \bar{M}_{\delta m} \sin(\varpi_\alpha t + \varphi_\alpha) \quad (71)$$

Assuming steady state conditions with the values of the random draws of current run, the amplitude of the sinusoidal pitch rate disturbance is about[‡] 1.5 mil.rad/sec , which, not surprisingly, is consistent with amplitude of the pitch control sinusoidal variation showed by Figure 16.

Figure 16 shows that while the control of the angle of attack has reached the steady state, the control of the pitch rate still exhibits, in the case of the Adaptive Continuous control, a (small) sinusoidal motion to compensate for the sinusoidal time varying pitch disturbance. Assuming steady state conditions $\delta_m \approx -M_\alpha \alpha / \bar{M}_{\delta m}$ hold and with the values of the random draws d_α, φ_α of the current run, the amplitude of the sinusoidal pitch rate disturbance is about 0.025 rad/sec that is commensurate with the disturbing effects.

Higher Order Sliding Mode Control is inherently insensitive to the matched disturbances as is the case here. The control compensates implicitly for the disturbing effects with a minor time lag due to the control law parasitic dynamics. This can be viewed in the zoomed plot of the pitch rate Figure 17.

The introduction of observers allows estimating “explicitly” the disturbing effects, providing that their dynamics is chosen to be much faster than the dynamics of the control. In this case the lag time will get reduced and, thus, a residual level of uncompensated disturbances is minimized. The combination of the explicit and implicit

compensation of the disturbance would be almost perfect should the design be proper. With fixed observers, the pitch rate exhibits some residual oscillations[§] as shown by Figure 17, where a corresponding residual level of uncorrected pitch rate oscillations is about $25 \mu\text{rad/sec}$; this level of residual oscillation is only 1/1000 of the initial disturbing effects, which is in itself a very good performance. The drawback is the chattering of the observer at a much faster frequency.

Continuous Adaptive HOSM control, as shown in Figure 17, can reduce the residual level of oscillations furthermore to an even smaller level of $5 \mu\text{rad/sec}$ amplitude. The use of the adaptive sliding mode observer has reduced the residual effects of the disturbing term from 25 mrad/sec to $5 \mu\text{rad/sec}$ and has eliminated the high frequency chattering.

5. Conclusion

This paper has presented two novel continuous Higher Order Sliding Mode (HOSM) autopilot designs driven by embedded HOSM observers applied to a hypersonic glider that must operate with uncertain or perturbed aerodynamics. The first design, used as reference, is Nonlinear Dynamic Sliding Manifold (NDSM based Second-order-Sliding Mode Controller (2-SMC)). The second and third designs modeled include respectively a fixed gain and adaptive gain HOSM observer aimed at reducing residual control chatter. Autopilot designs using NDSM designs have been proposed [23, 27], they achieve good performance. They are applicable to systems of relative degree smaller or equal 2, typically to track commanded angle of attack or pitch angle; unfortunately, they could not be used for integrated guidance and autopilots aimed at directly tracking a guidance variable^{**} such as the rotation of the LOS or the target relative velocity perpendicular to the LOS because corresponding relative degrees $r = 4$. Proposed Continuous or Adaptive HOSM controllers represent a technical breakthrough in that they are applicable to systems of arbitrary relative degree and thus, and, they could be used in integrated guidance and control algorithms. Results obtained first show the feasibility of such algorithms and their applicability to the control problem posed but, moreover, they achieve a slightly better performance than the already excellent performance of NDSM-based 2-SMC. Besides, Continuous Adaptive HOSM control achieves a very significant reduction of the control chattering as compared to fixed parameter observer design. The significant reduction of the residual level of pitch rate oscillations is conducive to alleviating vehicle vibrations. Finally, an impulsive controller (RCS) performs in a concert with Continuous HOSM designs. The purpose of such RCS/impulsive control is to

‡ The disturbance is multiplicative, that a sinusoidal variation of the value of the stability derivative of few percentage multiplied by a small value of the control

§ The lag which can be observed in Figure 17 would be between the “mean” of the Fixed-Gain continuous observer and the adaptive continuous HOSM: the first would be minimum at 2.7 sec. whereas the second would bottom at 2.75 sec.

** That is in a single layer control that does not include intermediate inversion algorithms

achieve rapidly a quasi dead-beat of the sideslip angle and rate in approximately $0.4 \text{ sec}^{\dagger\dagger}$. This control is aimed as remedying extraordinary situations where, due to the mediocre lateral stability and limited lateral control authority, the sideslip angle becomes uncontrollable as the sideslip angle may exceeds some critical magnitude. The proposed the hybrid continuous HOSM-Impulsive controller demonstrated excellent performance.

References

- [1] Parker J., Serrani A., Yurkovich S., Bolender M., Doman D. "Control-oriented modeling of an air-breathing hypersonic vehicle," *Journal of Guidance, Control, and Dynamics*, Vol. 30, No. 3, 2007, pp. 856–869, DOI: 10.2514/1.27830.
- [2] Fiorentini L., Serrani A., Bolender M. A., and Doman D. B., "Robust Nonlinear Sequential Loop Closure Control Design for an Air-breathing Hypersonic Vehicle Model," *Proceedings of American Control Conference*, 2008, pp. 3458-3463, DOI: 10.1109/ACC.2008.4587028.
- [3] Farwell, J., Sharma, M., Polycarpou, M., "Backstepping-Based Flight Control with Adaptive Function Approximation," *Journal of Guidance, Control, and Dynamics*, Vol. 28, No.6, 2005, pp. 1089–1102, DOI: 10.2514/1.13030.
- [4] Chen, W. H., "Observer Enhanced Dynamic Inversion of Missiles," *Journal of Guidance, Control, and Dynamics*, Vol. 25, No.1, 2002, pp. 161–166, DOI: 10.2514/2.5027
- [5] C. Tournes, Y. Shtessel, and I. Shkolnikov, "Autopilot for Missiles Steered by Aerodynamic Lift and Divert Thrusters Using Nonlinear Dynamic Sliding Manifolds," *AIAA Journal on Guidance, Control, and Dynamics*, Vol. 29, No. 3, (May-June), 2006, pp. 617-625, DOI: 10.2514/1.15486
- [6] A. Levant, "Quasi-continuous high-order sliding-mode controllers," *IEEE Trans. Automat. Control*, Vol. 50, No. 11, 2006, pp. 1812-1816, DOI: 10.1109/TAC.2005.858646
- [7] Y. Shtessel, C. Edwards, L. Fridman, and A. Levant, *Sliding Mode Control and Observation*, Birkhauser, Springer, New York, 2014, ISBN 978-0-8176-4893-0.
- [8] Levant, A. (Levantovsky, L. V.), "Sliding order and sliding accuracy in sliding mode control", *International Journal of Control*, Vol. 86, 1993, pp. 1247-1263, DOI: <https://doi.org/10.1080/00207179308923053>
- [9] A. Thukral and M. Innocenti, "Sliding Mode Missile Pitch Autopilot Synthesis for High angle of Attack Maneuvering," *IEEE transactions on Control Systems Technology*, Vol. 6, No. 3 1998, pp. 359-371, DOI: 10.1109/87.668037
- [10] Y. Shtessel, I. Shkolnikov and A. Levant, "Smooth Second Order Sliding Modes: Missile Guidance application," *Automatica*, Vol. 43, No.8, 2007, pp. 1470-1476, DOI: <https://doi.org/10.1016/j.automatica.2007.01.008>
- [11] P. Yu, Y. Shtessel, and C. Edwards, "Continuous Higher Order Sliding Mode Control with Adaptation of Air Breathing Hypersonic Missile," *Int. J. Adapt. Control Signal Process*, Vol. 30, Issues 8-10, August-October 2016, pp. 1099-1118, DOI: 10.1002/acs.2664.
- [12] W. Zhang, X. Huang, and X.-Z. Gao, "Dynamic output feedback H_∞ attitude control for hypersonic gliding vehicles," *International Journal of Innovative Computing, Information & Control*, Volume 13, Issue 4, pp. 1351-1368, 2017.
- [13] X. Yu, P. Li, and Y. Zhang, "The Design of Fixed-Time Observer and Finite-Time Fault-Tolerant Control for Hypersonic Gliding Vehicles," *IEEE Transactions on Industrial Electronics*, Volume 65, Issue 5, pp. 4135-4144, 2018.
- [14] G. Kumar, A. Sakar, and S. Talole, "Dynamic pressure based mid-course guidance scheme for hypersonic boost-glide vehicle," *Proceedings of the Institute of Mechanical Engineers, Part G: Journal of Aerospace Engineering*, Published online: August 24, 2018, <https://doi.org/10.1177/0954410018795265>
- [15] K. Zhao, D.-Q. Cao, and W.-H. Huang, "Maneuver control of the hypersonic gliding vehicle with a scissored pair of control moment gyros," *Science China Technological Sciences*, Volume 61, Issue 8, pp. 1150-1160, August 2018.
- [16] C. Edwards and Y. Shtessel "Adaptive Continuous Higher Order Sliding Mode Control," *Automatica*, Vol. 65, 2016, pp 183-190, DOI: <https://doi.org/10.1016/j.automatica.2015.11.038>
- [17] Bhat, S. P., and Bernstein, D. S., "Geometric homogeneity with applications to finite time stability", *Math. Control Signals Systems*, Vol. 17, 2005, pp. 101–127, DOI: <https://doi.org/10.1007/s00498-005-0151-x>
- [18] M. T. Angulo, J. A. Moreno and L. Fridman, "An Exact and Uniformly Convergent Arbitrary Order Differentiator," *Proceedings of CDC-ECC, Orlando*, 2011, pp.7629-7634, DOI:10.1109/CDC.2011.6160926
- [19] B. Miller and E. Rubinovich, *Impulsive Control in Continuous and Discrete- Continuous Systems*. Amsterdam: Kluwer Academic Publishers, 2002, DOI: 10.1007/978-1-4615-0095-7
- [20] Y. Orlov, *Discontinuous Systems: Lyapunov Analysis and Robust Synthesis Under Uncertainty Conditions*, Springer, London, 2008, ISBN 978-1-84800-984-4.
- [21] A. Levant, "Higher-order sliding modes, differentiation and output-feedback control". *International Journal of Control*, 76, 9/10, 2003, pp. 924-941, DOI: <https://doi.org/10.1080/0020717031000099029>.
- [22] F. M. Aldukali, and Y. B. Shtessel, "Continuous Higher Order Sliding Mode Control with Impulsive Action," *Proceedings of the Conference on Decision and Control*, Osaka, Japan, December 2015, DOI: 10.1109/CDC.2015.7403068.
- [23] Y. Shtessel, A. Glumineau, F. Plestan, and F. Aldukali, "Hybrid-impulsive second-order sliding mode control: Lyapunov approach," *International Journal on Robust and Nonlinear Control*, Volume 27, Issue 7, May 2017, pp. 1064–1093, DOI: 10.1002/rnc.3618.
- [24] M. Weiss and Y. Shtessel, "An Impulsive Input Approach to Short Time Convergence for Linear Systems," *Advances in Aerospace Guidance Navigation and Control*, Q. Chu, B. Mulder, D. Choukroun, E. van Kampen, C. de Visser and G. Looye (Eds.) Springer, July 2013, pp. 99-119, DOI https://doi.org/10.1007/978-3-642-38253-6_8, ISBN 978-3-642-38252-9.

$\dagger\dagger$ The 0.4 sec. time has been selected arbitrarily and assuming the practicality of the impulse thrusters, should corresponding level of thrust not be compatible with vehicle size, longer settling times should be considered

- [25] I. Gel'fand and G. Shilov, "Generalized functions," Academic Press, 1964, ISBN-10: 1-4704-2658-7.
- [26] Recommended Practice for Atmospheric Flight Vehicles Coordinate Systems, ANSI/AIAA R-004-1992.
- [27] Tournes, C., "Compendium of Flight Mechanics Formulae Applied to Hypersonic Gliders, AIAA Paper 2013 4609, Aug. 2013, DOI: 10.2514/6.2013-4609
- [28] Vallado, D., "Fundamentals of Astrodynamics and Application," Space Technology Library, El Segundo, CA, 2001, pp. 141-151, ISBN 1-881883-12-4
- [29] A. Tiwari, "Atmospheric and Space Flight Dynamics," Birkhauser, Springer, New York, 2006, pp. 53-289 ISBN-10:0-8176-4373-7
- [30] P. Faure, "Navigation Inertielle Optimale et Filtrage Statistique," Dunod, Paris, 1971, p. 268 (in French)
- [31] Stevens, B. L., Lewis, F. L., "Equations of Motion, "Aircraft Control and Simulation, Wiley, New York, 1992, pp. 1-48, ISBN 0-471-61397-5
- [32] Y. Shtessel, B. Chava, and C. Edwards, "Second Order Sliding Mode Control using Nonlinear Dynamic Sliding Manifold: Lyapunov Approach," Proceedings of the Conference on Decision and Control, Osaka, Japan, December 2015, DOI 10.1109/CDC.2015.7